Journal of Fluids and Structures (1998) **12,** 839–858
Article No. fl980174

LIMIT CYCLE BEHAVIOR OF AN AIRFOIL WITH A CONTROL SURFACE

D. Tang, E. H. Dowell And L. N. Virgin

School of Engineering, Duke University, Durham, NC 27708-0300, U.S.A.

(Received 11 September 1997 and in revised form 29 July 1998)

A three-degree-of-freedom aeroelastic model with freeplay is modeled theoretically using a small number of aerodynamic eigenmodes (i.e. a reduced order model) based upon Peters' finite-state model for two-dimensional aerodynamic flow. The limit cycle behavior and the sensitivity to initial conditions for the onset of limit cycle oscillations are discussed. A simple and interesting physical explanation for this behavior is presented based on harmonic balance or describing function calculations that have been confirmed by numerical time simulations. The theoretical results are also in good agreement with experiment and a universal scaling law for the dependence of limit cycle oscillations and bifurcation parameters on freeplay is elucidated.

1. INTRODUCTION

An earlier theoretical/experimental study of an aeroelastic wing system with a trailing-edge flap including structural freeplay has been presented in Conner, Tang, Dowell & Virgin (1997). Based on the nonlinear structural model presented in Conner *et al.* (1997), a reduced-order finite-state aerodynamic model based upon Peters' finite-state model, presented in Peters & Cao (1995) for the two-dimensional aerodynamic flow over an airfoil, has been applied to this nonlinear aeroelastic system in Tang, Conner & Dowell (1998). Using a small number of these aerodynamic eigenmodes (i.e. a reduced-order model), the aeroelastic model was formed by coupling them to a typical section structural model with a trailing edge flap and including a freeplay nonlinearity in flap rotation. A schematic of the typical airfoil section with a control surface at the trailing-edge of the main wing is shown in Figure 1(a) and a freeplay nonlinearity in the structural stiffness of the control surface is shown in Figure 1(b). Results obtained from the direct time integration of the nonlinear equations were shown by Tang *et al.* (1998) to be in good agreement with previous theoretical and experimental work of Conner *et al.* (1997).

In the present paper, we use an equivalent linearization technique often referred to as the "describing function" approach or harmonic balance method to analyze the nonlinear equations. The harmonic balance method provides additional physical insight, not readily obtainable from the earlier time simulations. Attention is focussed on the limit cycle behavior. The numerical results can be given a simple and interesting physical explanation that is confirmed by the time simulation of the nonlinear equations. The present study is a continuation and extension of Tang *et al.* (1998).

2. MATHEMATICAL MODEL

Using the reduced-order finite-state aerodynamic model, a nonlinear aeroelastic model can be described by the following system of nonlinear equations:

$$[M_e]\{\ddot{y}\} + [C_e]\{\dot{y}\} + [K_e]\{y\} + \{M_\beta\} - [B_m]\{\lambda_m^R\}\{q\} = \{0\} \tag{1}$$

0889-9746/98/070839 + 20 $30.00

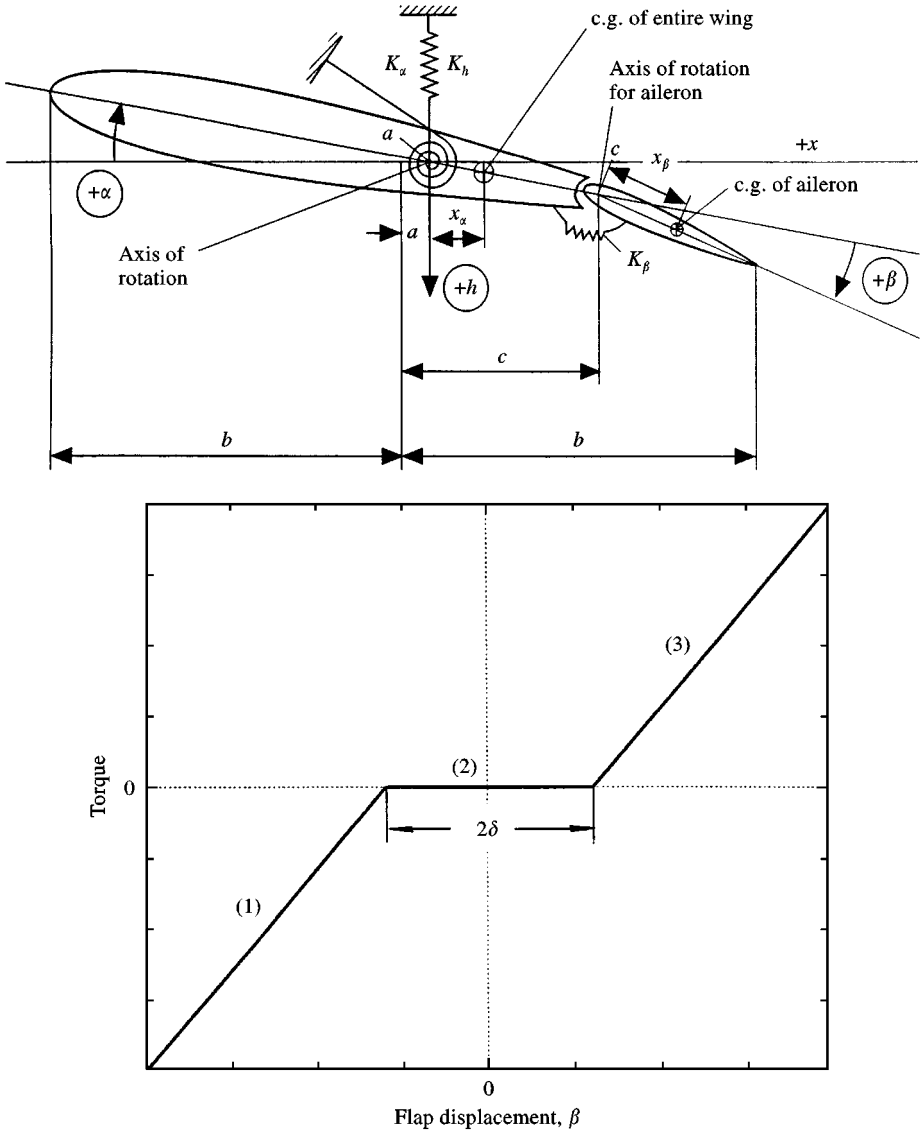

Figure 1. (a) Sketch of the aeroelastic typical section with control surface. (b) Restoring moment due to K_β with a symmetric freeplay region about $\beta = 0$.

and

$$\{\dot{q}\} + \frac{U}{b}[\Lambda]\{q\} - [\lambda_m^{\mathrm{L}}]^{\mathrm{T}}([B_1]\{\ddot{y}\} + \frac{U}{b}[B_2]\{\dot{y}\}) = \{0\}.$$

Let $\{X\} = \{y, q\}^{\mathrm{T}}$, equation (1) can be written as a compact matrix equation

$$[M_x]\{\ddot{X}\} + [C_x]\{\dot{X}\} + [K_x]\{X\} = -\{M_\beta\}, \tag{2}$$

where

$$[M_x] = \begin{bmatrix} M_e & 0 \\ -(\lambda_m^{\mathrm{L}})^{\mathrm{T}} B_1 & 0 \end{bmatrix},$$

$$[C_x] = \begin{bmatrix} C_e & -\frac{U}{b}(\lambda_m^{\mathrm{L}})^{\mathrm{T}} B_2 \\ 0 & 1 \end{bmatrix},$$

$$[K_x] = \begin{bmatrix} K_e & -B_m \lambda_m^{\mathrm{R}} \\ 0 & \frac{U}{b}\Lambda \end{bmatrix},$$

and where $\{y\}$ is a structural response vector composed of $\{h, \alpha, \beta\}^{\mathrm{T}}$, with plunge directed by h, pitch by α and flap by β as degree of freedom. $\{q\}$ is the vector of modal coordinates of the finite-state aerodynamic model, $[\lambda^{\mathrm{R}}]$ and $[\lambda^{\mathrm{L}}]$ are the right and left aerodynamic eigenvector matrices, and Λ is a diagonal matrix whose diagonal entries contain the aerodynamic eigenvalues. B_m, B_1 and B_2 are aerodynamic coefficient matrices arising from the aerodynamic model, and M_e, C_e, K_e are equivalent mass, damping and stiffness matrices arising from the structural and aerodynamic models. More details of this aerodynamic modeling can be found in Tang *et al.* (1998).

With a structural freeplay gap, the control surface-restoring moment-rotation relationships may be expressed as

$$M_\beta = \begin{cases} K_\beta(\beta - \delta) & |\beta| \geq \delta,\ \beta > 0, \\ K_\beta(\beta + \delta) & |\beta| \geq \delta,\ \beta < 0, \\ 0 & \text{otherwise.} \end{cases} \tag{3}$$

TABLE 1
System parameters used in simulation

Geometry parameters	
Chord	0·254 m
Span	0·52 m
Semi-chord, b	0·127
Elastic axis a w/r/t b	−0·5
Hinge line c w/r/t b	0·5
Mass (*inertial*) *parameters*	
Mass of wing	0·62868 kg
Mass of aileron	0·18597 kg
Mass/length of wing-aileron	1·558 kg
(Mass of support blocks)	(0·47485 × 2 kg)
S_α (per span)	0·08587 kg m
S_β (per span)	0·00395 kg m
x_α	0·434
x_β	0·01996
I_α (per span)	0·01347 kg m^2
I_β (per span)	0·0003264 kg m^2
Stiffness parameters	
K_α (per span)	37·3 kg m/s^2
K_β (per span)	3·9 kg m/s^2
K_h (per span)	2818·8 kg/m/s^2
Damping parameters	
ζ_α (half-power)	0·01626
ζ_β (half-power)	0·0115
ζ_h (half-power)	0·0113
Frequency parameters	
ω_α (coupled)	9.21 Hz
ω_β (coupled)	19·44 Hz
ω_h (coupled)	4.45 Hz

The aeroelastic behavior of this system is significantly dependent upon the nonlinear flap stiffness which differs importantly from the nominal linear stiffness, K_β.

3. DESCRIBING FUNCTION APPROACH

If we assume a fundamental harmonic solution for the flap rotation of this nonlinear system,

$$\beta = \beta_s \sin \omega t,$$

then from equation (3) and the describing function or harmonic balance approach, an equivalent flap stiffness, $K_{\beta\mathrm{eq}}$, of the nonlinear flap rotation is determined as

$$K_{\beta\mathrm{eq}} = F_\delta K_\beta. \tag{4}$$

In this expression, F_δ is the describing function which accounts for the presence of the freeplay nonlinearity and, most significantly, depends upon the flap rotation. Using the describing function technique, we obtain a representation for the freeplay nonlinearity of the form (Hsu & Meyer 1968)

$$F_\delta = \begin{cases} 0 & -\delta < \beta_s < \delta, \\ \frac{1}{\pi}(\pi - 2t - \sin 2t) & \text{otherwise}, \end{cases} \tag{5}$$

where t is given by

$$t = \sin^{-1}(\delta/\beta_s).$$

If we use $K_{\beta\mathrm{eq}}\beta$ instead of the nonlinear term for M_β from equation (3), then equivalent linearized equations are obtained. Giving a value of $K_{\beta\mathrm{eq}}$, and solving the linearized equations, the flutter velocity, U_F, and flutter frequency, ω_F, can be determined as a function $K_{\beta\mathrm{eq}}$. Then, from a knowledge of $K_{\beta\mathrm{eq}}$ and K_β, F_δ is determined from equation (4) and β_s/δ from equation (5). Thus, U_F and ω_F are known as a function of flap amplitude, β. We can also obtain the plunge and pitch amplitudes from the now known β, using the harmonic balance method. The latter procedure is described as follows.

Let

$$\{X\} = \{X_s\} \sin \omega_F t + \{X_c\} \cos \omega_F t, \tag{6}$$

where $\{X_s\} = \{h_s, \alpha_s, \beta_s, q_{1s}, q_{2s}, \dots\}^{\mathrm{T}}$ and $\{X_c\} = \{h_c, \alpha_c, 0, q_{1c}, q_{2c}, \dots\}^{\mathrm{T}}$.

Substituting equations (3)–(6) into equation (2) and rearranging the matrix equations we have

$$\begin{bmatrix} K_x - \omega_F^2 M_x & \omega_F C_x \\ -\omega_F C_x & K_x - \omega_F^2 M_x \end{bmatrix} \begin{Bmatrix} X_c \\ X_s \end{Bmatrix} = - \begin{Bmatrix} K_{\beta\mathrm{eq}} \\ 0 \end{Bmatrix} \beta_s. \tag{7}$$

Note that equation (7) is a set of linear algebraic equations with the known variables, β_s and ω_F, and β_s is included in $\{X_s\}$.

Solving equation (7) we obtain

$$|\alpha(U)| = \sqrt{\alpha_s^2 + \alpha_c^2}, \qquad |h(U)| = \sqrt{h_s^2 + h_c^2}.$$

4. NUMERICAL RESULTS

4.1. RESULTS FOR THE LINEAR SYSTEM ($\delta = 0$)

Figure 2(a) shows the flutter velocities of the linear system versus the flap stiffness, K_β, from 0 to 2·05 kg m^2/s^2. (Note that 2·05 is the value for the experimental wind tunnel model and

also that the flutter boundary changes little for $K_\beta > 2{\cdot}05$.) There are two flutter velocities of special interest. One is $U_{F0} = 8{\cdot}6$ m/s which corresponds to $K_\beta = 0$ or $\omega_\beta = 0$ and the other is $U_{F\min} = 4.5$ m/s which corresponds to $K_\beta = 0{\cdot}1$ kg m^2/s^2 or $(\omega_\beta/\omega_\alpha)_{\min} = 0{\cdot}46$ [see Figure 2(b)] and is the minimum flutter velocity for all ω_β. Figure 2(b) shows the flutter

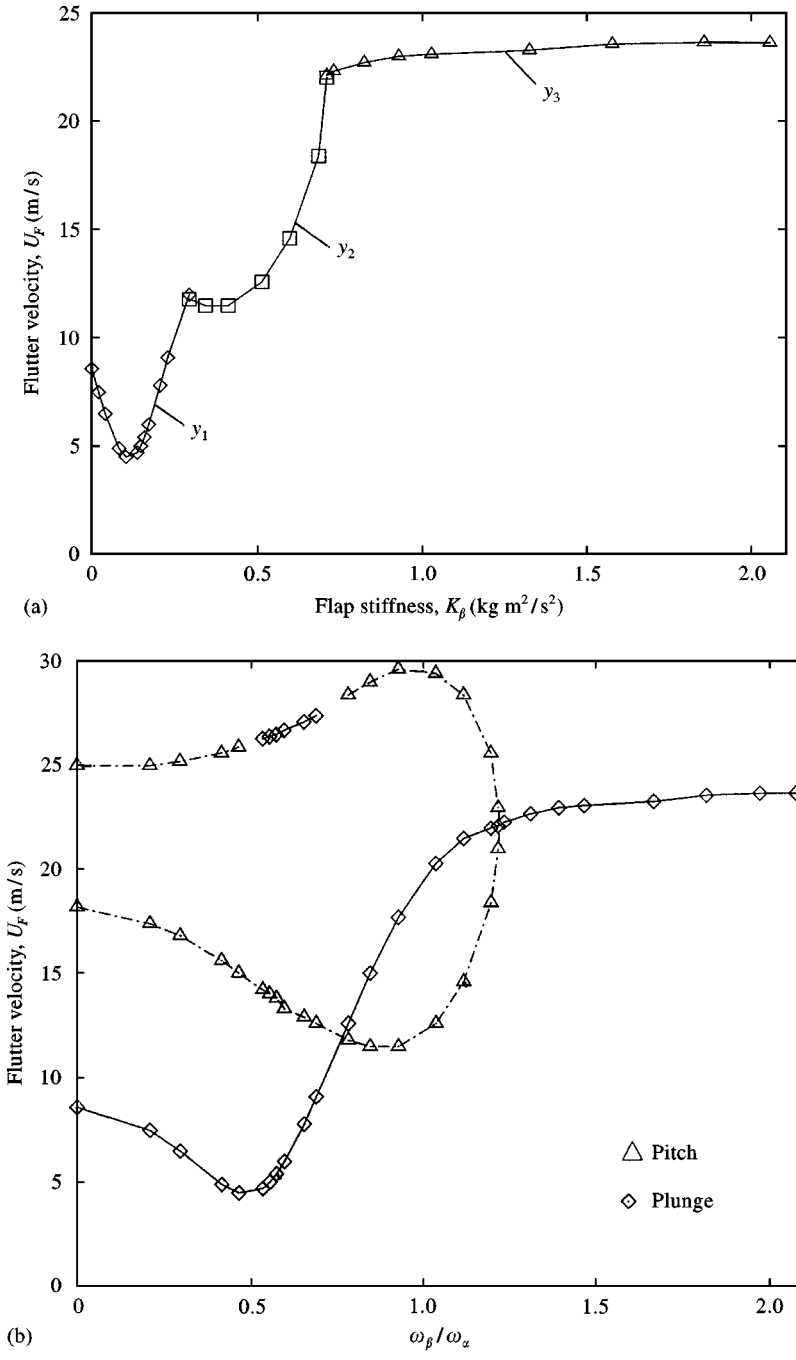

Figure 2. (a) Flutter velocity versus flap stiffness for the linear system; $M = 4$ aerodynamic states. (b) Flutter velocity versus $\omega_\beta/\omega_\alpha$ for the linear system. (c) Flutter frequency versus flap stiffness.

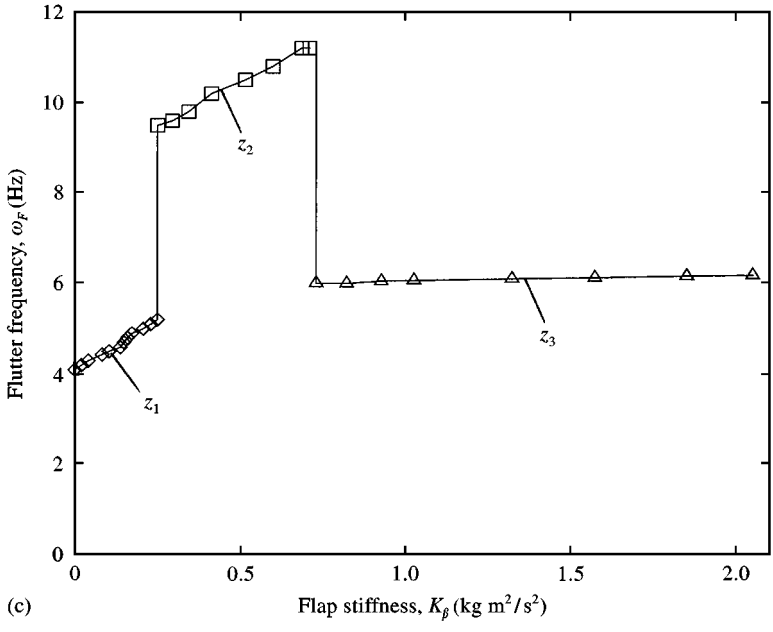

Figure 2. (*Continued*).

velocities of this linear system versus the uncoupled frequency ratio, $\omega_\beta/\omega_\alpha$. There is only one flutter velocity for $\omega_\beta/\omega_\alpha$ greater than 1·2, or $K_\beta > 0{\cdot}73\,\text{kg m}^2/\text{s}^2$. For $\omega_\beta/\omega_\alpha$ less than 1·2, there are two distinct flutter boundaries, one indicated by the symbol $\triangle$ and the other indicated by the symbol $\diamond$. Note that for the former ($\triangle$), there is a bounded range of flow velocity for which the motion is unstable. The lowest flutter velocity is the most critical, of course, and it is given by the branches of the curves denoted by y_1, y_2 and y_3 in Figure 2(a).

Figure 2(c) shows the flutter frequencies of this linear system versus the flap stiffness, K_β. Not surprisingly, we find there is an abrupt change in the flutter frequency at $K_\beta = 0{\cdot}29$, i.e. the frequency jumps to a high frequency (near the pitch natural frequency) from a low frequency (near the plunge natural frequency). At $K_\beta = 0{\cdot}7$, there is another abrupt change in the frequency from high to low. The flutter frequency branches in Figure 2(c) denoted by z_1, z_2 and z_3 correspond to branches y_1, y_2 and y_3 in Figure 2(a).

Figure 3(a–d) shows (a, b) the eigenvalue solutions of the linear system for $K_\beta = 0$, and (c, d) $K_\beta = 0{\cdot}2\,\text{kg m}^2/\text{s}^2$ or $\omega_\beta/\omega_\alpha = 0{\cdot}65$, with Figure 3 (a, c) showing the real part or damping and Figure 3 (b, d) the root-locus. The arrows indicate the direction of the loci when U increases. From Figure 3(a, b) we find that there are two intersections with the flow velocity axis for the nominal pitch motion and one intersection for the nominal plunge motion, and from Figure 3(c, d) there are two intersections with the flow velocity axis for the plunge motion and one intersection for the pitch motion. Note that, in fact, all motions in Figures 2 and 3 are truly coupled plunge, pitch and flap motions; so, to speak of purely plunge or pitch motion is not possible. The additional eigenvalues shown in these figures arise from the aerodynamic modes. Of course, strictly speaking all eigenvalues shown are coupled aerodynamic/structural, i.e. aeroelastic modes.

4.2. Results for the Nonlinear System ($\delta = \pm 2{\cdot}12^\circ$)

For the nonlinear system, a specific freeplay configuration was chosen corresponding to a nominal angular gap of $4{\cdot}24^\circ$, i.e. $\delta = \pm 2{\cdot}12^\circ$. However, as noted in Conner *et al.* (1997) and Tang *et al.* (1998), all responses scale in proportion to δ. The calculations are based

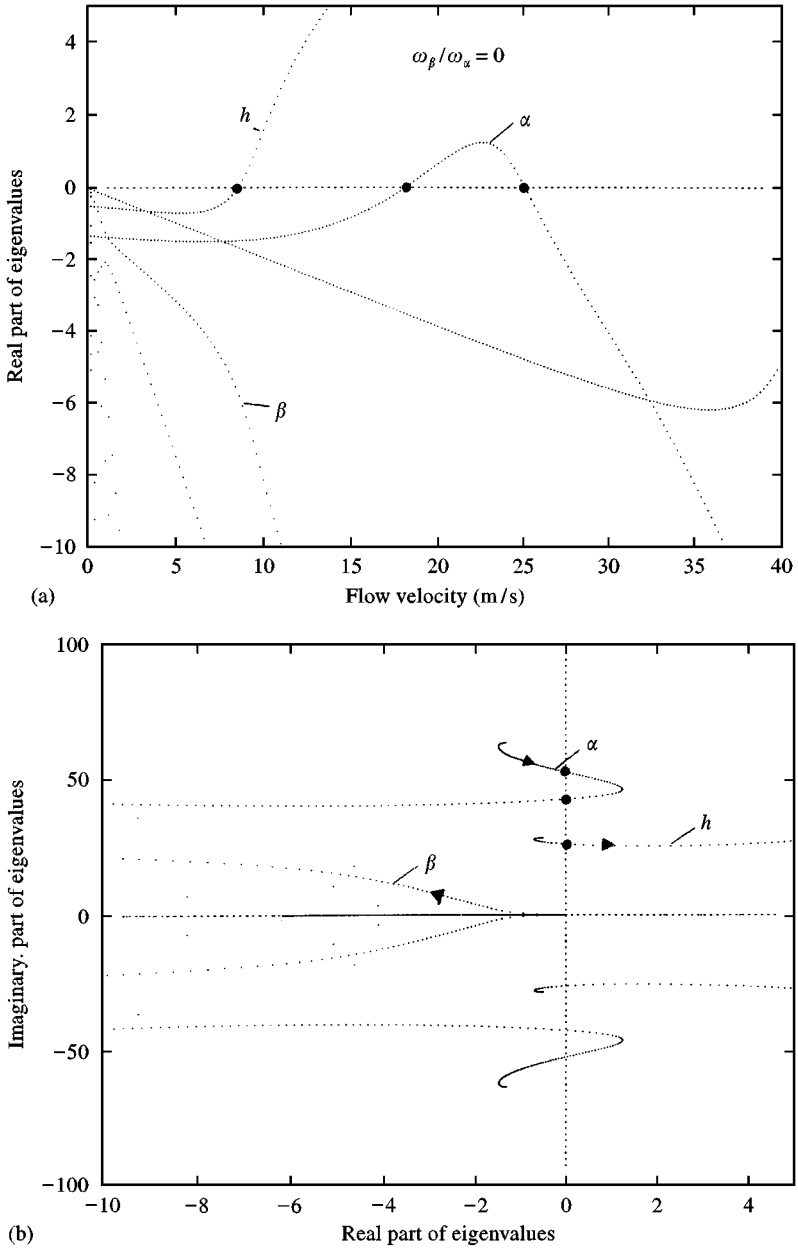

Figure 3. Eigenvalue solutions of the linear system for using reduced order model with $M = 4$: (a, b) for $\omega_\beta/\omega_\alpha = 0$; (c, d) for $\omega_\beta/\omega_\alpha = 0{\cdot}65$, (a, c) show the real part of the eigenvalues and (b, d) the root-locus. The arrows indicate the direction of motion of the loci when U increases.

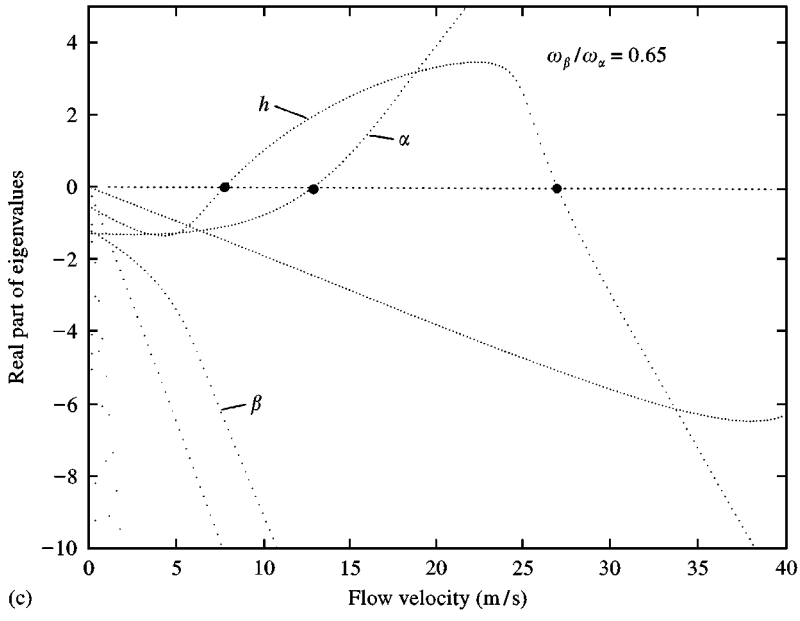

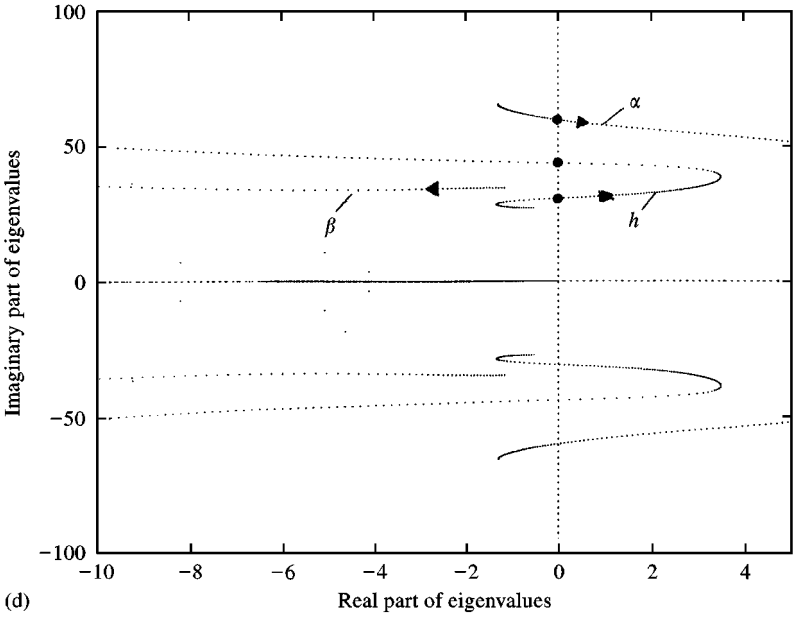

Figure 3. (*Continued*).

upon the describing function or harmonic balance approach (assuming a single harmonic) and confirmed by nonlinear numerical time simulations with a reduced-order aerodynamic model of $M = 4$. The numerical response data points corresponding to periodic behavior are given for a peak amplitude normalized by the angular gap, and the corresponding velocities are normalized by U_{F0}. Note that this normalization is different from that

used in Conner *et al.* (1997) and Tang *et al.* (1998) for reasons that will become clear in what follows.

In this paper, attention is focussed on two typical cases. One is for a higher flap stiffness that is greater than the pitch stiffness, i.e., $\omega_\beta/\omega_\alpha = 2{\cdot}1$. The other is for a lower flap stiffness with $\omega_\beta/\omega_\alpha = 0{\cdot}65$.

4.2.1. *Results for* $\omega_\beta/\omega_\alpha = 2{\cdot}1$

Employing equations (3) and (4), the relationship between the nondimensional equivalent stiffness, $K_{\beta\mathrm{eq}}/K_\beta$, and the nondimensional flap rotation β/δ may be obtained. This relationship is shown in Figure 4 as a function of the nondimensional flap amplitude. For β/δ less than one, the equivalent stiffness is zero. As the amplitude increases, the magnitude of $K_{\beta\mathrm{eq}}$ approaches that of K_β.

From the linear flutter equations (when $M_\beta = K_{\beta\mathrm{eq}}\beta$), equation (1), a relationship between the equivalent stiffness, $K_{\beta\mathrm{eq}}$, and the flutter velocity, U_F, is determined as in Figure 2(a). From Figures 4 and 2(a), the nondimensional flap amplitude of the limit cycle oscillation (LCO) versus the nondimensional flow velocity, $\bar{u} = U_F/U_{F0}$, can be determined as shown in Figure 5. The stable flap LCO is indicated by the solid line, and the unstable LCO by the symbol ●. There are two unstable LCO branches, the first one between $\bar{u} = 0{\cdot}52$ and 1 has a frequency near the plunge natural frequency and the second one between $\bar{u} = 1{\cdot}34$ and $1{\cdot}4$ has a frequency near the pitch natural frequency. Results from the time integration of nonlinear equation (1) indicated by the dashed line and the experimental results indicated by the symbols □ are also plotted in this figure. It is found that four distinct regions of response behavior can be observed. First, up to about $\bar{u} = 0{\cdot}5$, there is a static equilibrium only. Here any initial disturbance dies out. For a flow rate slightly

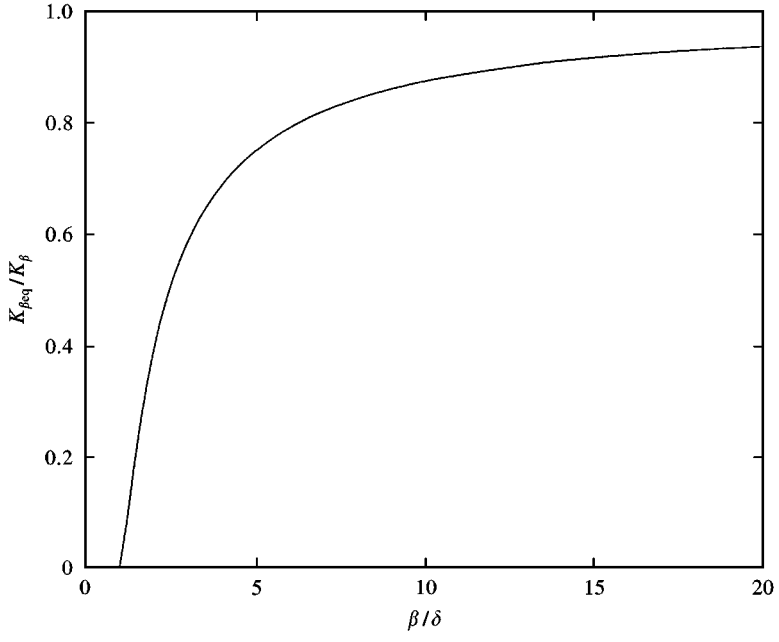

Figure 4. Nondimensional equivalent flap stiffness for the freeplay nonlinearity.

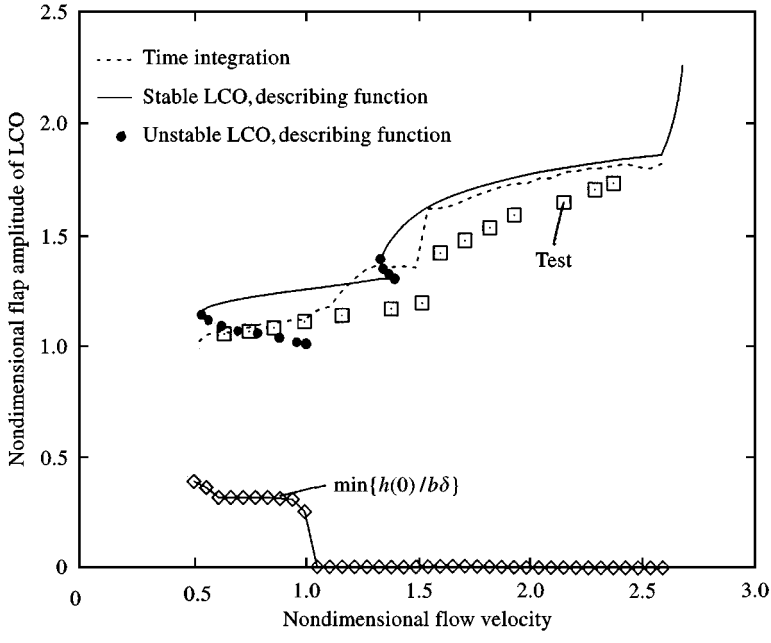

Figure 5. Nondimensional flap amplitude of limit cycle oscillation versus nondimensional flow velocity, $\bar{u}$, for $\omega_\beta/\omega_\alpha = 2{\cdot}1$.

greater than $\bar{u} = 0{\cdot}5$, there is a discrete jump to a low-frequency limit cycle. At about $\bar{u} = 1{\cdot}5$ there is another abrupt change in the system response. The low-frequency limit cycle becomes unstable (rather suddenly) and a high-frequency limit cycle response occurs. The flap amplitude has a relatively small increase with the change in LCO. However, this new LCO is characterized by a sudden drop in the plunge amplitude, as shown in Figure 6(a). The pitch response is shown in Figure 6(b). It is seen that the theoretical results from the nonlinear time integration and describing function approaches show good correlation and also good correlation with experiment. For $\bar{u} > 2{\cdot}52$, the response has a very large amplitude as $\bar{u}$ approaches the linear flutter velocity for $\omega_\beta/\omega_\alpha = 2{\cdot}1$ and the oscillation frequency approaches the plunge natural frequency. Tests were not conducted for this range, in order to preclude the possibility of damage to the experimental model.

Both the describing function and time integration approaches suggest that for flow velocities between $U = U_{F0}$ and $U_{F\min}$ or $\bar{u} = 0{\cdot}5$ to $1{\cdot}0$, a finite disturbance is required to excite the LCO while for $\bar{u} > 1{\cdot}0$ or $U > U_{F0}$, the LCO will be excited for any infinitesimal disturbance. The minimum finite initial conditions required to excite the LCO can only be determined by time integration, and the minimum initial plunge displacements required to excite the LCO are shown in Figures 5 and 6.

This limit cycle behavior described above has a simple and interesting physical explanation, as follows. With freeplay, the flap frequency is really a function of the amplitude of response, varying between zero when the motion is small and within the freeplay range and increasing to the nominal flap frequency when the motion is large and extending well beyond the freeplay range. Now *linear* theory predicts that the flutter velocity has a minimum for some value of flap frequency. If that flap frequency is between zero and the nominal value, then flutter *may* occur for velocities above the minimum flutter velocity

predicted by linear theory and, indeed, the minimum flutter velocity for the present example is $\bar{u} = 0{\cdot}52$. From *nonlinear* theory, one may determine the magnitude of the initial disturbance required to initiate such a flutter limit cycle. It turns out that the magnitude of the initial disturbance required to initiate the limit cycle is smallest in the plunge degree of freedom. (See Figure 6(c); note that this figure uses a logarithmic scale.) In fact, the value is

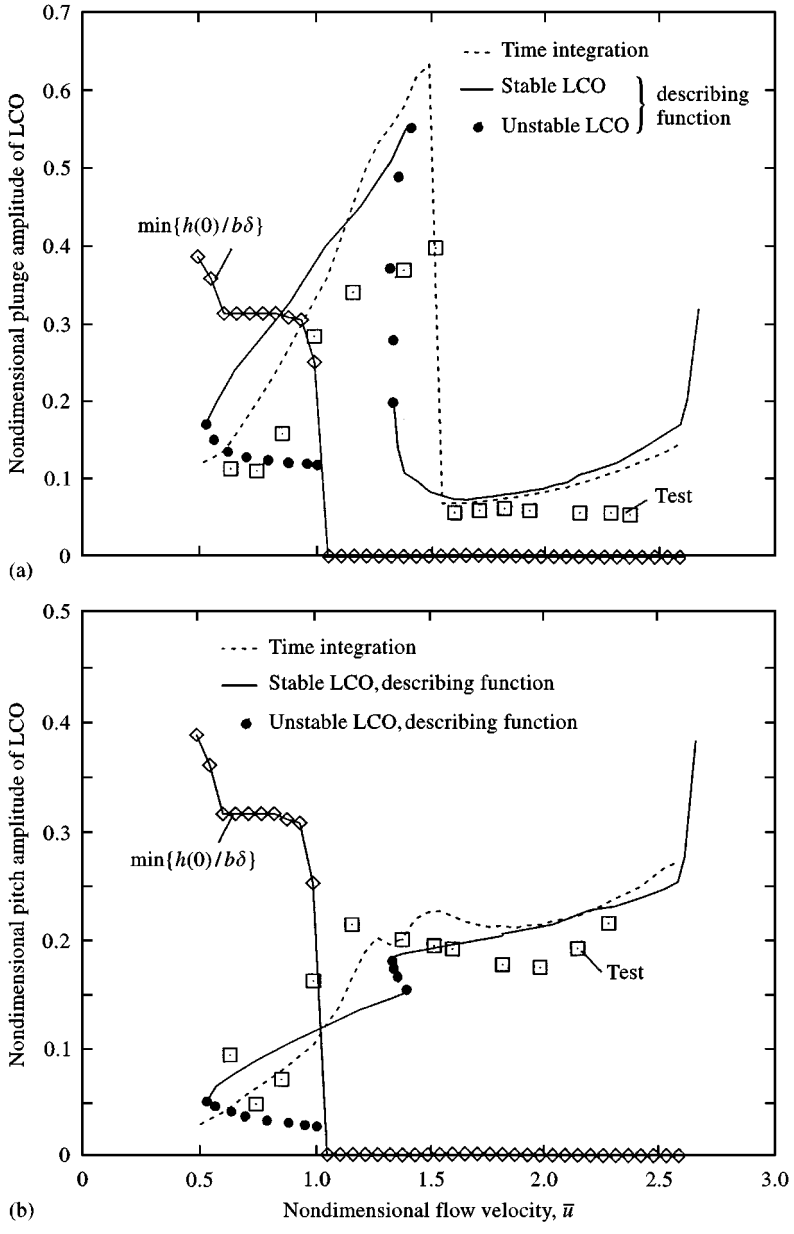

Figure 6. Nondimensional response amplitude of limit cycle oscillation and initial condition values versus nondimensional flow velocity, $\bar{u}$, for $\omega_\beta/\omega_\alpha = 2{\cdot}1$: (a) for plunge (b) for pitch. (c) Minimum initial conditions in plunge, pitch and flap, respectively, required to initiate LCO.

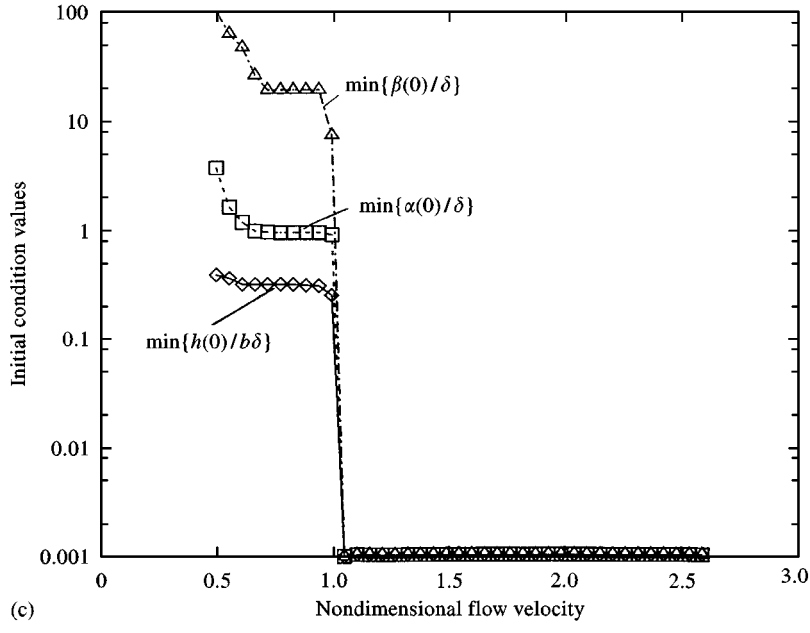

Figure 6. (*Continued*).

quite small in physical terms, $h/\delta b \sim 0{\cdot}3$. For typical δ, the amplitude of the plunge initial displacement required to initiate the limit cycle is no more than 1% of the airfoil half-chord, b. Thus, in our experiments, we were able to apply a small disturbance in the plunge degree of freedom to readily excite the limit cycle.

If the nominal flap frequency is decreased, the theory suggests that a larger initial disturbance is required to excite the limit cycle below the flutter velocity predicted by linear theory for zero flap frequency. This observation explains the difference in results between those reported for our experimental model and those described by Lacabanne & Humbert (1997) for an experimental model with a flap frequency well below the pitch frequency. Also see the discussion in Section 4.2.2 that follows.

Figure 7(a–c) shows time histories of the limit cycle oscillations of the flap rotation, (a) for $U/U_{F0} = 0{\cdot}74$, (b) for $U/U_{F0} = 1{\cdot}35$ and (c) for $U/U_{F0} = 2{\cdot}0$. The dashed line is for the present results, the dotted line is for the theoretical results given by Conner & Dowell (1997) and the solid line for the experiment. At the lower flow velocity, $\bar{u} = 0{\cdot}74$, the LCO is near the plunge natural frequency. At the higher velocity, $\bar{u} = 2{\cdot}0$, the LCO is near the pitch natural frequency. At the middle velocity, $\bar{u} = 1{\cdot}35$, a subharmonic response occurs. In Figure 8, a FFT analysis of the flap rotation is shown for $U/U_{F0} = 0{\cdot}74$, 1·35 and 2·0. Note that the motion is more nearly simple harmonic for the larger values of U/U_{F0}, which is consistent with the closer agreement between the results from harmonic balance and time integration in this velocity range, as seen in Figures 5 and 6.

4.2.2. *Results for* $\omega_\beta/\omega_\alpha = 0{\cdot}65$

Figure 9 shows the nondimensional flap amplitude of the LCO and the minimum plunge initial condition values that lead to limit cycle oscillations versus the nondimensional flow

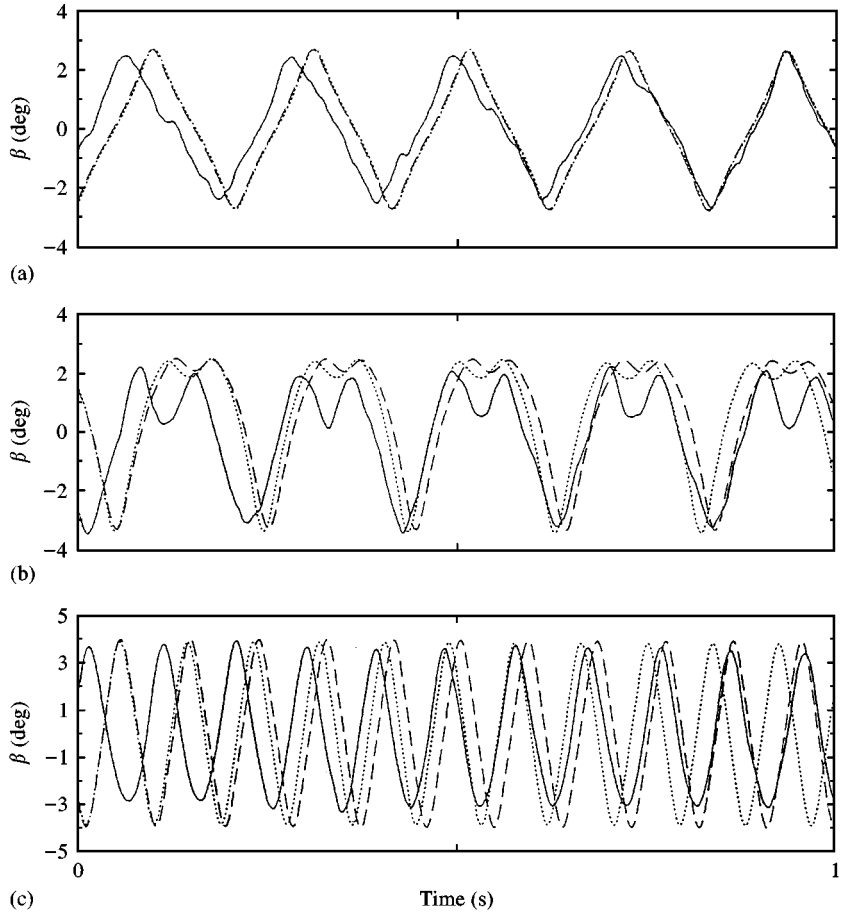

Figure 7. Limit cycle oscillations of flap rotation, response for $\omega_\beta/\omega_\alpha = 2{\cdot}1$: (a) for $\bar{u} = 0{\cdot}74$; (b) for $\bar{u} = 1{\cdot}35$; (c) for $\bar{u} = 2{\cdot}0$; ——, reduced order model with $M = 4$; … Conner *et al.* (1997); —, experiment.

velocity, $\bar{u}$. Again, there are two flow velocities of special interest: $U = 4{\cdot}44$ m/s or $\bar{u} = 0{\cdot}51$, corresponds to the lowest value for which a limit cycle may occur for a sufficiently large initial condition and $U = 8{\cdot}58$ m/s or $\bar{u} = 1{\cdot}0$ corresponds to the value above which a limit cycle occurs for any initial plunge disturbance.

Figure 10(a–c) show the nondimensional plunge and pitch amplitudes of LCO and the minimum initial condition values for the onset of the limit cycle oscillation versus the nondimensional flow velocity for: (a) the plunge response, (b) the pitch response, and (c) the minimum initial condition values required to initiate LCO. Note that a logarithmic scale is used in Figures 9 and 10.

Figure 11(a–d) shows the time histories of limit cycle oscillation for $U/U_{F0} = 0{\cdot}55$: (a) plunge for $t = 0 \rightarrow 50$ s, (b) plunge for the last one second (from a record of 49–50 s), (c) pitch and (d) flap rotation. A FFT analysis of the flap motion for $U/U_{F0} = 0{\cdot}55$ and $0{\cdot}75$ is shown in Figure 12. A single harmonic oscillation near the plunge natural frequency is evident. This explains the excellent agreement between the results from time integration and harmonic balance analysis for this $\omega_\beta/\omega_\alpha$.

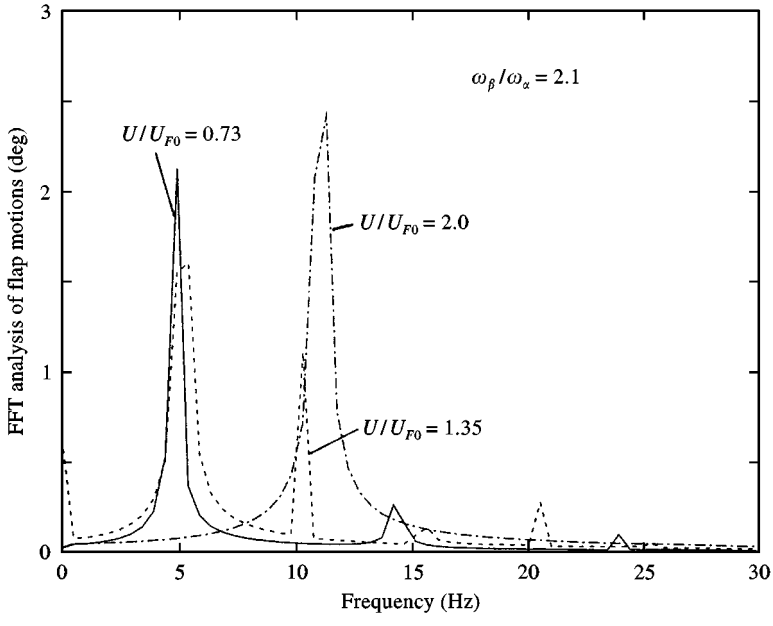

Figure 8. FFT analysis of the flap rotation for $\bar{u} = 0{\cdot}73$, $1{\cdot}35$ and $2{\cdot}0$.

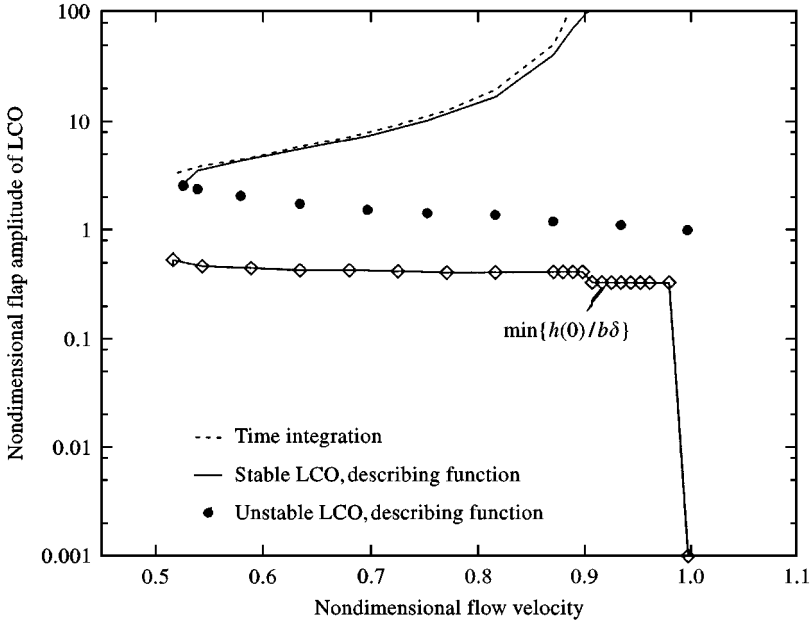

Figure 9. Nondimensional flap amplitude of limit cycle oscillation versus nondimensional flow velocity, $\bar{u}$, for $\omega_\beta/\omega_\alpha = 0{\cdot}65$.

4.2.3. *Results for other $\omega_\beta/\omega_\alpha$ values*

Figure 13 shows the nondimensional flap amplitude of the LCO versus the nondimensional flow velocity, $\bar{u}$, for $\omega_\beta/\omega_\alpha = 0$, 0·23, 0·46, 1·0, 4·2 and 8·4, calculated from the describing function approach. The results for $\omega_\beta/\omega_\alpha = 0{\cdot}65$ and 2·1 are also plotted in this figure. The

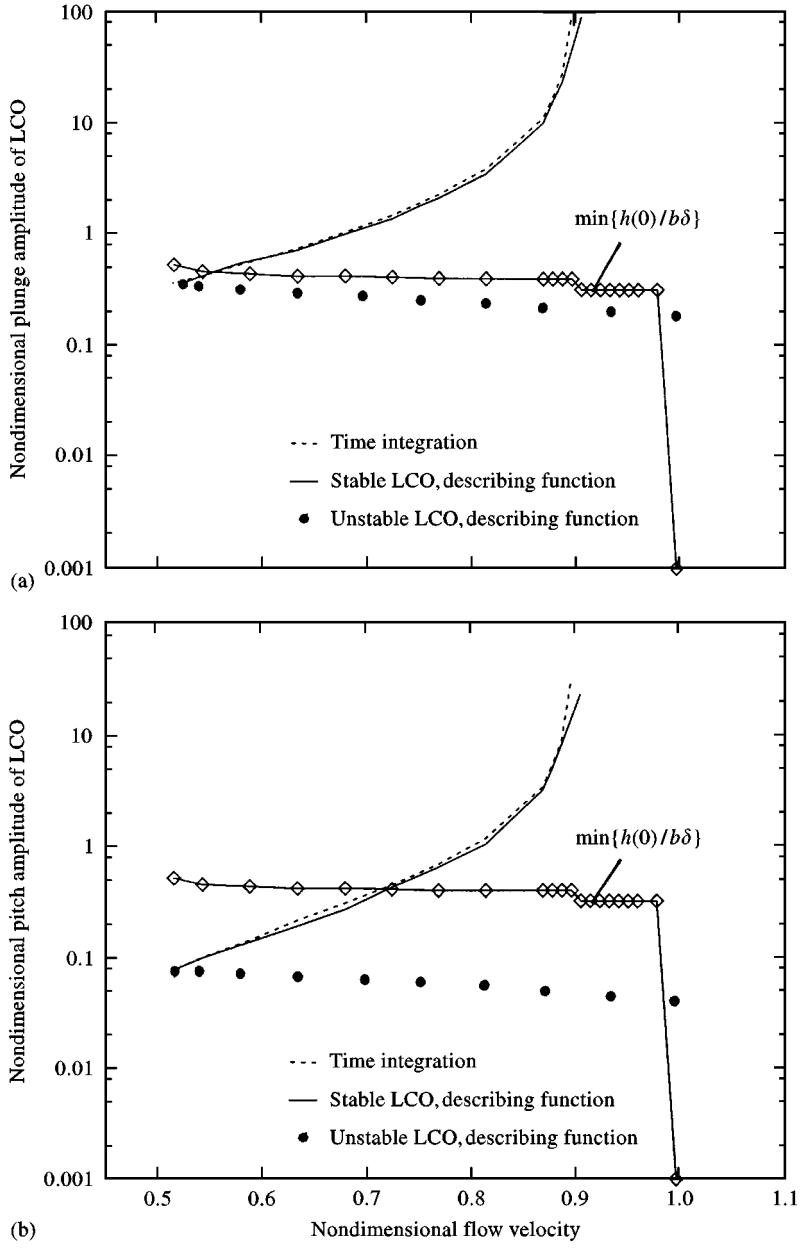

Figure 10. Nondimensional response amplitude of limit cycle oscillation and initial condition values vs nondimensional flow velocity, $\bar{u}$, for $\omega_\beta/\omega_\alpha = 0{\cdot}65$, (a) for plunge; (b) for pitch; (c) for initial conditions.

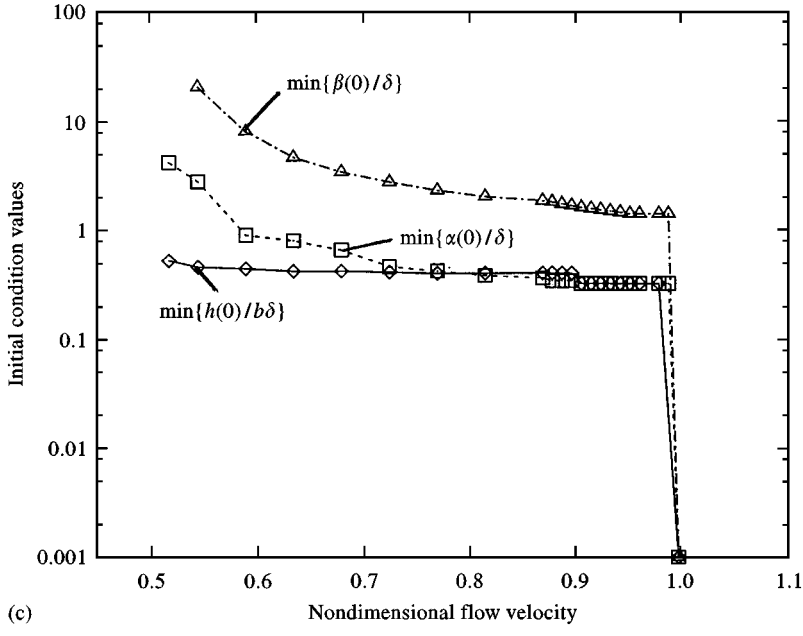

Figure 10. (*Continued*).

symbols indicate an unstable LCO and the solid line indicates a stable LCO. It is seen that for $\omega_\beta/\omega_\alpha \leqslant (\omega_\beta/\omega_\alpha)_{\min} = 0{\cdot}46$, no stable limit cycle oscillations have been found. Note that for $\omega_\beta/\omega_\alpha = 0{\cdot}0$, the result is a vertical line at $\bar{u} = 1$. When $\omega_\beta/\omega_\alpha > 0{\cdot}46$, the amplitude of the stable LCO decreases as $\omega_\beta/\omega_\alpha$ increases. A common characteristic of the LCO is that they have an unstable LCO between $\bar{u} = 0{\cdot}51$ and $1{\cdot}0$ and, for $\omega_\beta/\omega_\alpha > 0{\cdot}46$, between $\bar{u} = 1{\cdot}34$ and $1{\cdot}4$. This might have been anticipated from Figures 2(a, b). Note that, as $\omega_\beta/\omega_\alpha \to \infty$, the LCO amplitude, β/δ, approaches unity until the flow velocity reaches the linear flutter velocity, when $\beta/\delta \to \infty$.

There is an unstable LCO branch for all $\omega_\beta/\omega_\alpha$, and for $\omega_\beta/\omega_\alpha < (\omega_\beta/\omega_\alpha)_{\min}$ ($\equiv 0{\cdot}46$ for the parameters considered in the paper), there is *only* an unstable branch. Note that this value of $(\omega_\beta/\omega_\alpha)_{\min}$ and the bifurcation values of U_{F0}, $U_{F\min}$ and $U_{F\text{linear}}$ are all independent of δ as well. The parameter ω_α/ω_h (or equivalently ω_β/ω_h) has *not* been varied in this study. For most $\omega_\alpha/\omega_h > 1$, we expect similar qualitative behavior for the LCO, and indeed we expect this to be true also for $\omega_\alpha/\omega_h < 1$, with the roles of the pitch and plunge modes interchanged.

This critical value of $\omega_\beta/\omega_\alpha = 0{\cdot}46$ is that which gives the minimum flutter velocity for the linear system, see Figure 2(b). This is also the minimum velocity for which LCO may exist for the nonlinear system with freeplay for *any* $\omega_\beta/\omega_\alpha$.

5. CONCLUSIONS

With freeplay in the flap motion of a three-degree-of-freedom typical airfoil section, a variety of limit cycle oscillation behavior is observed. Experimental results show good agreement with the results from numerical time simulations and also from the describing function approach. The latter analysis provided a simple and interesting

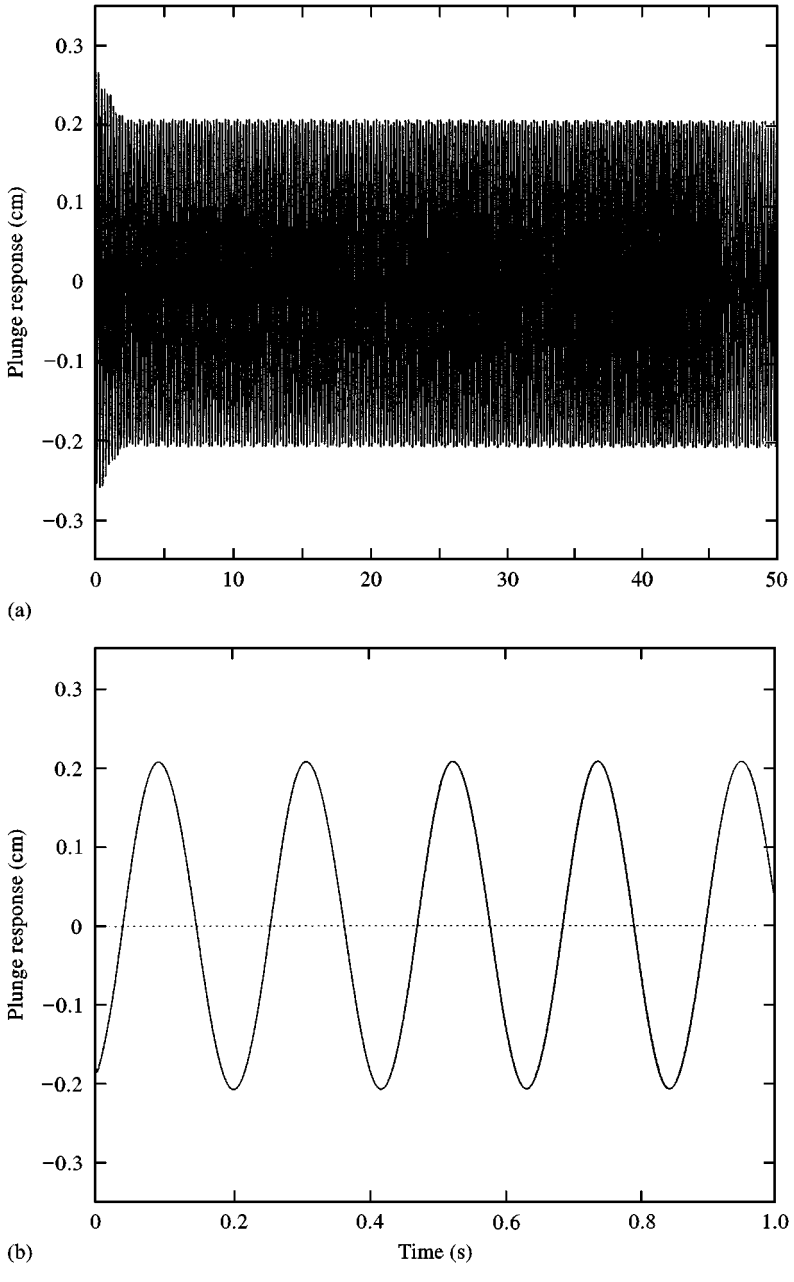

Figure 11. Time histories of limit cycle oscillations for $\omega_\beta/\omega_\alpha = 0{\cdot}65$ and $\bar{u} = 0{\cdot}55$: (a) for plunge response of $t = 1$–50 s; (b) for plunge response of $t = 49$–50 s; (c) for pitch response of $t = 49$–50 s (d) for flap response of $t = 49$–50 s.

physical explanation for the observed flutter limit cycle behavior and sensitivity to initial conditions.

Specifically, the harmonic balance has confirmed the conclusions of Conner *et al.* (1997) that the bifurcation velocities where limit cycle oscillations (LCO) occur are independent of the freeplay range. In addition, unstable LCO have been more easily identified and their

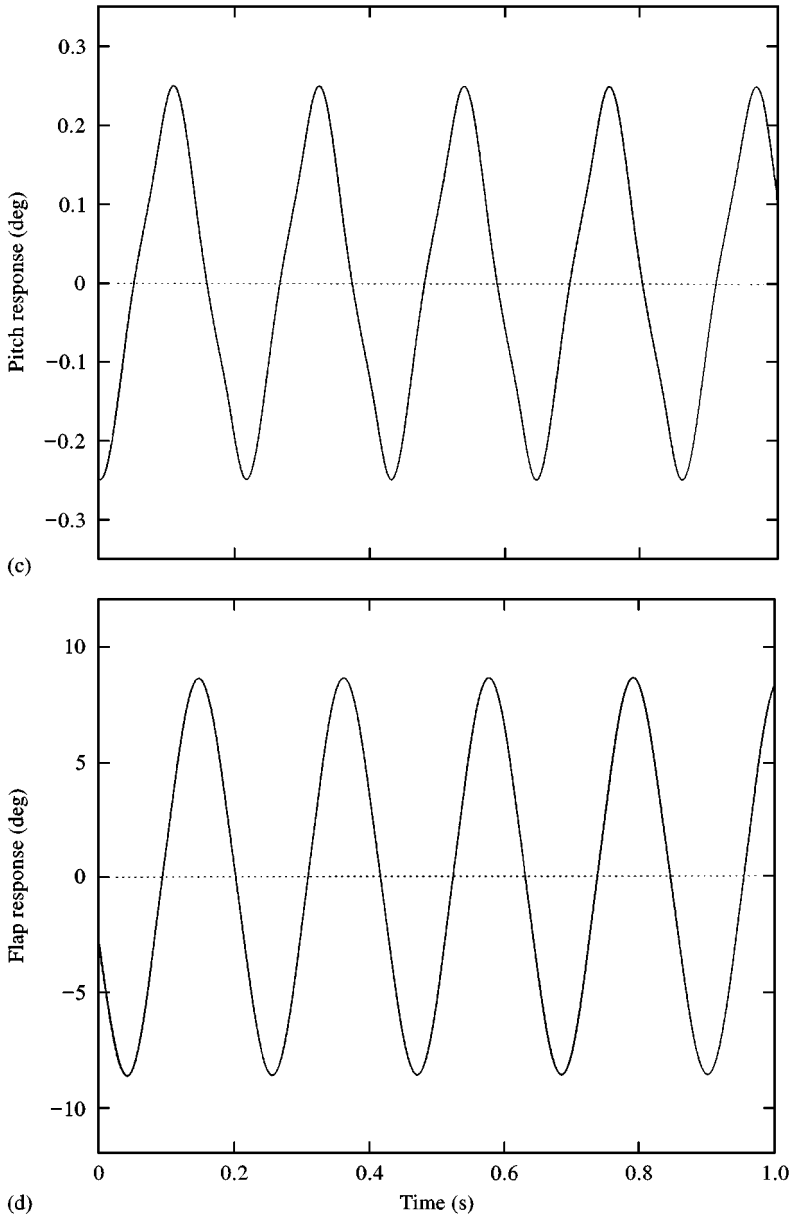

Figure 11. (*Continued*).

relationship to the effect of initial conditions better understood. Finally, and very importantly, the harmonic balance solution has suggested that the minimum velocity for which a LCO may occur (in the language of nonlinear dynamics this is a turning point where a stable and unstable LCO come together), for *any* ratio of nominal flap to pitch frequency, $\omega_\beta/\omega_\alpha$, and for *any* freeplay, corresponds to the minimum flutter velocity for the linear system *without* freeplay and with $\omega_\beta/\omega_\alpha$ allowed to assume the value that minimizes the flutter velocity.

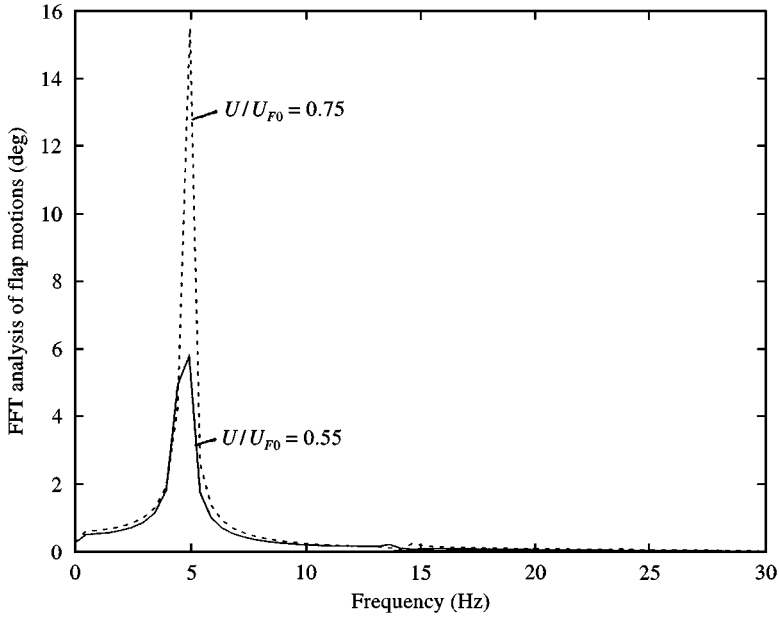

Figure 12. FFT analysis of the flap rotation for $\omega_\beta/\omega_\alpha = 0{\cdot}65$ and $\bar{u} = 0{\cdot}55$, $0{\cdot}75$.

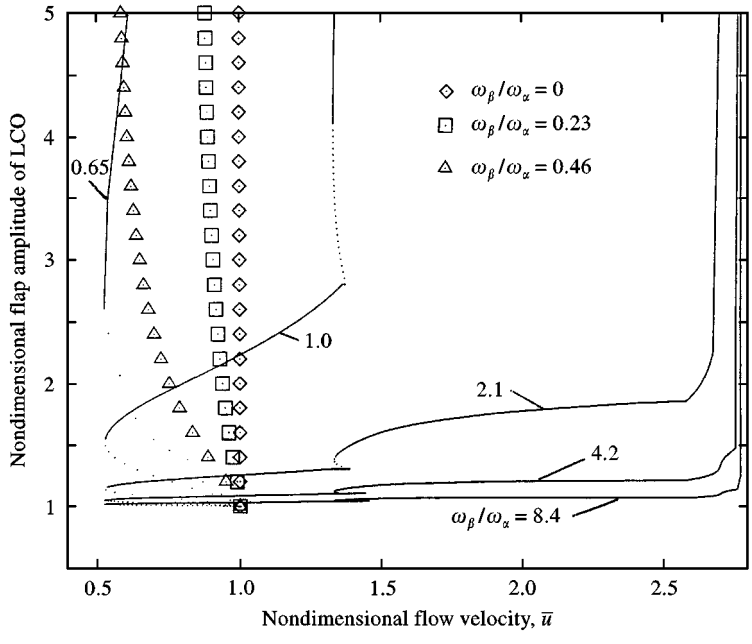

Figure 13. Nondimensional flap amplitude of limit cycle oscillation vs nondimensional flow velocity, $\bar{u}$, for $\omega_\beta/\omega_\alpha = 0$, $0{\cdot}23$, $0{\cdot}46$, $0{\cdot}65$, $1{\cdot}0$, $2{\cdot}1$, $4{\cdot}2$ and $8{\cdot}4$. The solid line denotes a stable LCO; the symbols (⊡, △ and ◇) denote unstable LCO.

ACKNOWLEDGMENT

This work was supported by the Air Force Office of Scientific Research under Grant F49620-97-1-0063. Major Brian Sanders is the technical monitor.

References

Conner, M. D., Tang, D. M., Dowell, E. H. & Virgin, L. N. 1997 Nonlinear behavior of a typical airfoil section with control surface freeplay: a numerical and experimental study. *Journal of Fluids and Structures*, **11,** 89–109.

Peters, D. A. & Cao, W. M. 1995 Finite state induced flow models; part I: two-dimensional thin airfoil. *Journal of Aircraft* **32,** 313–322.

Tang, D. M., Conner, M. C. & Dowell, E. H. 1998 Reduced order finite-state airloads and its applications to a nonlinear aeroelastic system. *Journal of Aircraft*, **35,** 332–338.

Hsu, J. C. & Meyer, A. V. 1968 *Modern Control Principles and Application*, Chapter 6. New York: McGraw-Hill.

Lacabanne, M. & Humbert, M. 1997 An experimental analysis of the aeroelastic behavior with a freeplay in a control surface. *Proceedings of the International Forum on Aeroelasticity and Structural Dynamics* (ed. L. Morino, 17–20 June, Rome, Italy, pp. 239–246.

APPENDIX: NOMENCLATURE

b	semi-chord of the airfoil section, $c/2$
c	chord of the airfoil section
F_{δ_c}	describing function corresponding to the freeplay nonlinearity
h	plunge displacement
$\bar{h}$	h/b
K_β	flap stiffness
$K_{\beta\mathrm{eq}}$	equivalent flap stiffness
M	size of reduced order aerodynamic model
M_β	flap moment about the flap axis
q	aerodynamic modal coordinate
t	time
U	air speed
U_F	linear flutter velocity
U_{F0}	linear flutter velocity corresponding to $K_\beta = 0$
$\bar{u}$	nondimensional flutter velocity, $\bar{u} = U_F/U_{F0}$
α	torsional angle of wing
β	flap rotational angle
δ	freeplay region
Λ	aerodynamic eigenvalue matrix
λ^{R}, λ^{L}	right and left aerodynamic eigenvector matrices
λ_m^{R}, λ_m^{L}	reduced order right and left eigenvector matrices with m aerodynamic modes
ρ	air density
ω_h, ω_α	plunge and torsional natural frequencies
ω_β	flap natural frequency
ω_F	flutter frequency
$(')$	d( )/dt
$(\ )_s$, $(\ )_c$	sine and cosine components of the variables h, α, β and q